



www.sciencemag.org/cgi/content/full/334/6052/79/DC1

Supporting Online Material for

A Self-Quenched Defect Glass in a Colloid-Nematic Liquid Crystal Composite

T. A. Wood, J. S. Lintuvuori, A. B. Schofield, D. Marenduzzo, W. C. K. Poon*

*To whom correspondence should be addressed. E-mail: w.poon@ed.ac.uk

Published 7 October 2011, *Science* **334**, 79 (2011)

DOI: 10.1126/science.1209997

This PDF file includes:

Materials and Methods

SOM Text

Figs. S1 to S4

Full Reference List

Materials and Methods

Experiments

We used polymethylmethacrylate (PMMA) particles loaded with 7-nitrobenzo-2-oxa-1,3-diazole-methyl methacrylate (NBD) (30) and sterically stabilized by chemically grafted poly-12-hydroxystearic acid (PHSA) (31). Their diameter, $2a$, from dynamic light scattering were 0.7, 1.2 and $2.0\mu\text{m}$ (polydispersity $\approx 5\%$). Stock dispersions were vacuum dried at 50°C for at least 3 days and stored dry for up to a year. Before dispersing in liquid crystal (LC) the powder was again vacuum dried overnight at 50°C . The thermotropic nematic LC 4-*n*-pentyl-4'-cyanobiphenyl (5CB, Nematel) was used as purchased, and has a transition temperature of 35.2°C (32).

The volume fraction of a known mass of particle-LC mixture was calculated from the particle volume $\frac{4}{3}\pi a^3$ and the densities of 5CB and PMMA ($1\text{g}/\text{cm}^3$ and $1.188\text{g}/\text{cm}^3$ respectively). Dispersion at room temperature was achieved by repeated ultrasonication (10 minutes), whirlly mixing (5 minutes) and manual stirring until there was no further visual changes.

To confirm homotropic alignment of the LC (33), we performed polarization microscopy on single particles in a dilute sample sandwiched between glass plates treated to promote parallel alignment of the nematic director along the surface. Clean glass and cover slides were covered with the 1% aqueous solution of poly(vinyl alcohol) (98% hydrolyzed, $M_w = 13000 - 23000$, Sigma-Aldrich) and spun at 3000 rpm for 60 s using a spin coater (Cammax Pricema). After vacuum drying at 120°C for 30 minutes the coated glass was firmly rubbed along one direction with a velvet cloth. A drop of a dilute ($\phi \sim 0.1\%$) particle-LC mixture was dropped onto the glass slide and covered with the cover slide such that rub direction was oriented in the same direction as for the base glass slide.

Polarization imaging was performed in a Nikon Eclipse E800 microscope using a $100\times$ oil-immersion objective lens, with the polarizer aligned with the rub direction of the sample cell.

Between crossed-polars, we see a symmetric four-lobed pattern (34), consistent with quadrupolar distortion of the director for homeotropic anchoring at the particle surface. No ‘Saturn-ring’ defect line was observed, either because of poor spatial resolution for small particles, or because the particle supports a ‘Surface-ring’ defect. Confocal imaging at $100\times$ was performed using a Biorad Radiance 2100 scan head mounted on a Nikon TE300 microscope, with fluorescence excited at 488 nm and emitted 514 nm.

Rheometry was performed using a TA Instruments AR2000 controlled-stress rheometer at 20°C in a cone-plate geometry (1° , diameter 40 mm, $32\mu\text{m}$ truncation gap). Spin-coating the surfaces with a monolayer of the same particles as used in the bulk samples following by sintering at 100°C for 90 minutes minimized slip, as confirmed by simultaneous imaging (35). Samples with $\phi \gtrsim 45\%$ took many hours to relax under compression after the geometry was filled. Where the geometry was under-filled the moduli were normalised for the filled area. Measurements were only commenced when the normal stress $N \ll 0.01 \text{ Pa}$.

Simulations

Equations of motion and simulation methodology

We used a finite difference scheme to study the motion of particles (size $2a$) in a nematic LC. Our algorithm couples a molecular dynamics for the colloidal particle to a relaxational dynamics for the LC, which tends to minimize a free energy density (see below). Colloid surfaces impose normal anchoring on the LC director field, and the force acting on the colloidal particles, \mathbf{f}^{el} , includes an elastic contribution due to the director field distortion; the latter is computed by integrating the thermodynamic stress tensor $\Pi_{\alpha\beta}$ over the surface of the colloid:

$$f_\alpha^{\text{el}} = \int dS \nu_\beta \Pi_{\alpha\beta} \quad (\text{S1})$$

where ν is normal to the colloidal surface, S . The force acting on the particles also has a random contribution and a potential forbidding interpenetration. The colloids obey overdamped

dynamics. The purely relaxational dynamics of the LC does not capture hydrodynamic effects.

The Landau-de Gennes free energy \mathcal{F} which we use to describe the relaxational dynamics of the LC, is expressed in terms of a second-rank symmetric and traceless tensorial order parameters, \mathbf{Q} , and has bulk (\mathcal{F}_1) and distortion (\mathcal{F}_2) contributions,¹

$$\mathcal{F}_1 = \frac{A_0}{2} \left(1 - \frac{\gamma}{3}\right) Q_{\alpha\beta}^2 - \frac{A_0\gamma}{3} Q_{\alpha\beta} Q_{\beta\gamma} Q_{\gamma\alpha} + \frac{A_0\gamma}{4} (Q_{\alpha\beta}^2)^2, \quad (\text{S2})$$

$$\mathcal{F}_2 = \frac{K_1}{2} (\partial_\gamma Q_{\alpha\beta})^2 + \frac{K_2}{2} (\partial_\beta Q_{\alpha\beta})^2, \quad (\text{S3})$$

where, A_0 is a constant, γ controls the magnitude of order (equivalent to temperature or concentration for thermotropic and lyotropic LCs respectively), while $K_{1,2}$ are two elastic constants. Most of the simulations are performed in the one elastic constant approximation, $K_2 = 0$, and further tuning K_1 to be the average of the splay, bend and twist elastic constant for 5CB. If we take $2a = 10$, our typical simulation parameters translate into $0.3 \mu\text{m}$ size colloid with $\sim 10 \text{ pN}$ elastic constants (see below for more details on mapping simulations to experiments).

The anchoring of the director field on a boundary surface to a chosen director \hat{n}^0 is ensured by adding a surface term

$$f_s = \frac{1}{2} W_0 (Q_{\alpha\beta} - Q_{\alpha\beta}^0)^2 \quad (\text{S4})$$

$$Q_{\alpha\beta}^0 = S_0 (n_\alpha^0 n_\beta^0 - \delta_{\alpha\beta}/3), \quad (\text{S5})$$

where W_0 controls the anchoring strength and S_0 determines the degree of the surface order. If the surface order is equal to the bulk order, S_0 should be taken equal to q , the order parameter in the bulk (3/2 times the largest eigenvalue of the \mathbf{Q} tensor).

The relaxation equation of motion for \mathbf{Q} is taken to be (36)

$$\partial_t \mathbf{Q} = \Gamma \mathbf{H} \quad (\text{S6})$$

¹Here and hereafter Greek indices denote cartesian components and the summation convention applies.

where Γ is a collective rotational diffusion constant, and \mathbf{H} is the molecular field, i.e. the derivative of the free energy with respect to the order parameter \mathbf{Q} , made traceless.

Finally, the stress tensor $\Pi_{\alpha\beta}$ is:

$$\Pi_{\alpha\beta} = -\partial_\alpha Q_{\gamma\nu} \frac{\delta \mathcal{F}}{\delta \partial_\beta Q_{\gamma\nu}}. \quad (\text{S7})$$

Parameter mapping to physical units

To relate simulations to experiments, we need to calibrate length, energy and time scales (37, 38). In simulation units (SU), the lattice parameter ℓ and time step Δt are both unity. The length scale is fixed by the colloid diameter, which we take as 300 nm; this is slightly smaller than in our experiments, but leads to more efficient computations. In our simulations we set the size of the particle to be 10ℓ , i.e. $\ell \equiv 30$ nm. We next fix the energy scale by setting $A_0 = 10^5$ Pa, giving an elastic constant² of 0.167 SU $\equiv 7.52$ pN. Finally, we assign a value to the rotational viscosity to fix the time unit. Taking $\Gamma = 0.5$ SU and a real rotational viscosity of 0.1 Poise, we find that 1 time unit translates into 0.1 μ s.

Supporting text

Intracluster dynamics, free energy barriers and percolating defect networks

To show that non-percolating clusters, Fig. 4B, are held in place by LC elasticity, we have monitored the trajectories of one of the particles in a cluster, for a time of 10 ms, both in the presence and in the absence of an underlying LC host. The latter gives standard Brownian motion, while the former gives a tightly ‘caged’ trajectory, Fig. S1.

To estimate the energy barriers against particle dispersal in nematic LC, we have calculated

²This holds for the Landau-de Gennes elastic constant K . For $\gamma = 3$ which we use, this corresponds to a value for the Frank elastic constants equal to ~ 3.76 pN.

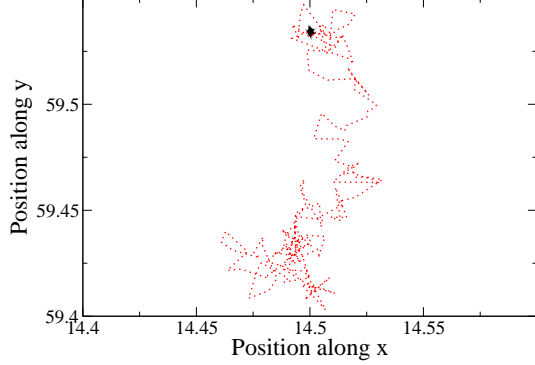


Figure S1: Trajectories of a 300 nm sphere in a cluster over a time of 10 ms at colloidal volume fraction of 7.3%. The black and red trajectories correspond to systems in the presence and absence of a liquid crystalline host, respectively. The positions are measured in simulation units.

the potential of mean force between two particles embedded in LC by performing a series of simulations in which the particles were held fixed at prescribed distances, with their center-to-center vector perpendicular to the far field nematic director field so that the optimal conformation is at contact, and allowing the LC to equilibrate via Eq. 6, whereupon the system's energy is the minimum at that inter-particle separation. By subtracting the energy at large separation, we obtain Fig. S2. There is a deep minimum when the particles touch (with an ‘entangled point defect’ configuration), and a small maximum at ~ 0.5 SU, giving a barrier of $\sim 168 k_B T$ with the parameters chosen here, but is generically of order $\sim 10^2 k_B T$ for other parameter values within a reasonable range for our experiments.

To clarify the details of the defect network, we replot the snapshot shown in Fig. 4C without the colloids in Fig. S3A. This shows the percolating defect network spanning the full length of the simulation box. At larger ϕ , the network becomes denser, with multiple branching points connecting the percolating defect network (Fig. S3B).

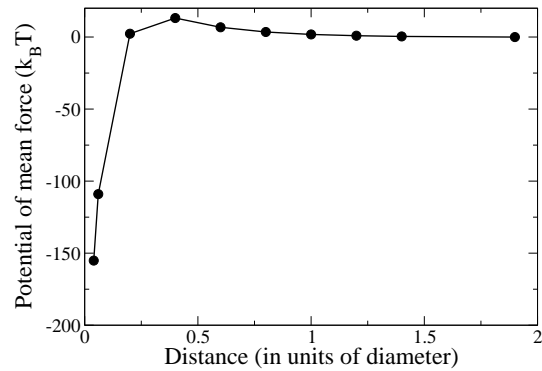


Figure S2: Plot of the potential of mean force versus relative surface-to-surface separation (normalized by particle diameter) for two colloidal particles in a nematic liquid crystal. The center-to-center vector is perpendicular to that of the far field nematic director.

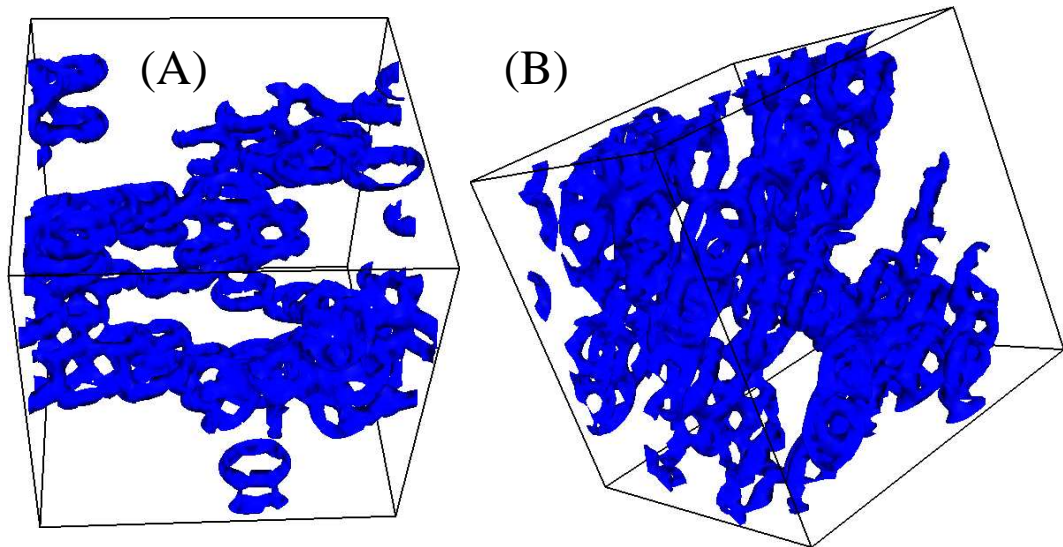


Figure S3: (A) Replot of Fig. 4C with colloids removed for clarity and (B) percolating defect network at $\phi \approx 23\%$.

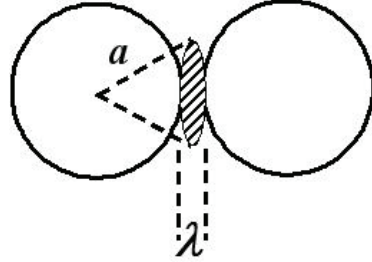


Figure S4: A volume of thickness λ between two defect-entangled particles (radius a) contains a nearly close-packed density of disclination lines.

Estimating the storage modulus

Here we give a geometric argument to estimate the elastic modulus of a suspension of particles at $\phi \sim 0.64$ entangled by defects. Consider two entangled particles, Fig. S4. The volume between particles, hatched, contains defects at the density of ≈ 1 per ℓ_c^2 , with modulus $G'_{\text{local}} \approx K/\ell_c^2$. Using the Derjaguin approximation, this volume is $a\lambda^2$. At random close packing of the particles, the fraction of the volume occupied by these defect-laden regions is $\psi \sim a\lambda^2/a^3 = (\lambda/a)^2$.

Since the load bearing is concentrated in these regions, a macro-strain applied to the whole sample, γ_{macro} , becomes a (magnified) local strain of $\gamma_{\text{local}} \sim (a/\lambda)\gamma_{\text{macro}}$. Finally, the macroscopic storage modulus is estimated by equating the elastic deformation energy stored at the macro- and micro-levels:

$$G'_{\text{macro}}\gamma_{\text{macro}}^2 = G'_{\text{local}}\gamma_{\text{local}}^2\psi, \quad (\text{S8})$$

$$\Rightarrow G'_{\text{macro}} \sim \frac{K}{\ell_c^2}, \quad (\text{S9})$$

which is independent of particle size.

Rough measurements from confocal micrographs suggest an interparticle spacing of ~ 1.1 times the particle diameter, so that $\lambda \sim 0.1a$. At high ϕ we observed a yield strain of $\gamma_{\text{macro}} \sim 10^{-3}$. This converts to $\gamma_{\text{micro}} \sim 10\gamma_{\text{macro}}$. Our observed (macro-)yield strain at high

ϕ of $\gamma_c \sim 10^{-3}$ therefore translates to a local yield strain of $\sim 10^{-2}$, which is equivalent to a movement of $\sim \ell_c \sim 5$ nm over a particle radius $a \sim 500$ nm, which should be enough to cause yielding of the material.

References

1. E. M. Herzig, K. A. White, A. B. Schofield, W. C. K. Poon, P. S. Clegg, Bicontinuous emulsions stabilized solely by colloidal particles. *Nat. Mater.* **6**, 966 (2007).
[doi:10.1038/nmat2055](https://doi.org/10.1038/nmat2055) [Medline](#)
2. P. Poulin, H. Stark, T. C. Lubensky, D. A. Weitz, Novel colloidal interactions in anisotropic fluids. *Science* **275**, 1770 (1997). [doi:10.1126/science.275.5307.1770](https://doi.org/10.1126/science.275.5307.1770) [Medline](#)
3. U. Tkalec, M. Ravnik, S. Čopar, S. Žumer, I. Mušević, Reconfigurable knots and links in chiral nematic colloids. *Science* **333**, 62 (2011). [doi:10.1126/science.1205705](https://doi.org/10.1126/science.1205705) [Medline](#)
4. P. G. de Gennes, J. Prost, *The Physics of Liquid Crystals* (Oxford Univ. Press, Oxford, 1995).
5. S. K. Pal, A. Agarwal, N. L. Abbott, Chemically responsive gels prepared from microspheres dispersed in liquid crystals. *Small* **5**, 2589 (2009). [doi:10.1002/smll.200900961](https://doi.org/10.1002/smll.200900961) [Medline](#)
6. A. Agarwal, E. Huang, S. Palecek, N. L. Abbott, Optically responsive and mechanically tunable colloid-in-liquid crystal gels that support growth of fibroblasts. *Adv. Mater.* **20**, 4804 (2008). [doi:10.1002/adma.200800932](https://doi.org/10.1002/adma.200800932)
7. S. J. Woltman, G. D. Jay, G. P. Crawford, Liquid-crystal materials find a new order in biomedical applications. *Nat. Mater.* **6**, 929 (2007). [doi:10.1038/nmat2010](https://doi.org/10.1038/nmat2010) [Medline](#)
8. T. Araki, M. Buscaglia, T. Bellini, H. Tanaka, Memory and topological frustration in nematic liquid crystals confined in porous materials. *Nat. Mater.* **10**, 303 (2011).
[doi:10.1038/nmat2982](https://doi.org/10.1038/nmat2982) [Medline](#)
9. E. H. Brandt, The flux-line lattice in superconductors. *Rep. Prog. Phys.* **58**, 1465 (1995).
[doi:10.1088/0034-4885/58/11/003](https://doi.org/10.1088/0034-4885/58/11/003)
10. M. J. Bowick, L. Chandar, E. A. Schiff, A. M. Srivastava, The cosmological kibble mechanism in the laboratory: String formation in liquid crystals. *Science* **263**, 943 (1994).
[doi:10.1126/science.263.5149.943](https://doi.org/10.1126/science.263.5149.943) [Medline](#)
11. H. Stark, Physics of colloidal dispersions in nematic liquid crystals. *Phys. Rep.* **351**, 387 (2001). [doi:10.1016/S0370-1573\(00\)00144-7](https://doi.org/10.1016/S0370-1573(00)00144-7)
12. R. W. Ruhwandl, E. M. Terentjev, Long-range forces and aggregation of colloid particles in a nematic liquid crystal. *Phys. Rev. E* **55**, 2958 (1997). [doi:10.1103/PhysRevE.55.2958](https://doi.org/10.1103/PhysRevE.55.2958)
13. I. Mušević, M. Škarabot, Self-assembly of nematic colloids. *Soft Matter* **4**, 195 (2008).
[doi:10.1039/b714250a](https://doi.org/10.1039/b714250a)
14. O. Guzmán, E. B. Kim, S. Grollau, N. L. Abbott, J. J. de Pablo, Defect structure around two colloids in a liquid crystal. *Phys. Rev. Lett.* **91**, 235507 (2003).
[doi:10.1103/PhysRevLett.91.235507](https://doi.org/10.1103/PhysRevLett.91.235507) [Medline](#)
15. T. Araki, H. Tanaka, Colloidal aggregation in a nematic liquid crystal: Topological arrest of particles by a single-stroke disclination line. *Phys. Rev. Lett.* **97**, 127801 (2006).
[doi:10.1103/PhysRevLett.97.127801](https://doi.org/10.1103/PhysRevLett.97.127801) [Medline](#)
16. M. Ravnik *et al.*, Entangled nematic colloidal dimers and wires. *Phys. Rev. Lett.* **99**, 247801 (2007). [doi:10.1103/PhysRevLett.99.247801](https://doi.org/10.1103/PhysRevLett.99.247801) [Medline](#)

17. V. J. Anderson, E. M. Terentjev, S. P. Meeker, J. Crain, W. C. K. Poon, Cellular solid behaviour of liquid crystal colloids 1. Phase separation and morphology. *Eur. Phys. J. E* **4**, 11 (2001). [doi:10.1007/PL00013680](https://doi.org/10.1007/PL00013680)
18. A. G. Chmielewski, E. Lepakiewicz, Rheological properties of some biphenyl liquid crystals. *Rheol. Acta* **23**, 207 (1984). [doi:10.1007/BF01332076](https://doi.org/10.1007/BF01332076)
19. A. Mertelj, M. Čopič, Observation of thermal fluctuations of disclination lines in a nematic liquid crystal. *Phys. Rev. E* **69**, 021711 (2004). [doi:10.1103/PhysRevE.69.021711](https://doi.org/10.1103/PhysRevE.69.021711) [Medline](#)
20. L. M. Walker, N. J. Wagner, R. G. Larson, P. A. Mirau, P. Moldenaers, The rheology of highly concentrated PBLG solutions. *J. Rheol.* **39**, 925 (1995). [doi:10.1122/1.550624](https://doi.org/10.1122/1.550624)
21. J. D. Bunning, T. E. Faber, P. L. Sherrell, The Frank constants of nematic 5CB at atmospheric pressure. *J. Phys.* **42**, 1175 (1981). [doi:10.1051/jphys:019810042080117500](https://doi.org/10.1051/jphys:019810042080117500)
22. L. Benguigui, Experimental study of the elastic properties of a percolating system. *Phys. Rev. Lett.* **53**, 2028 (1984). [doi:10.1103/PhysRevLett.53.2028](https://doi.org/10.1103/PhysRevLett.53.2028)
23. M. Zapotocky, L. Ramos, P. Poulin, T. C. Lubensky, D. A. Weitz, Particle-stabilized defect gel in cholesteric liquid crystals. *Science* **283**, 209 (1999). [doi:10.1126/science.283.5399.209](https://doi.org/10.1126/science.283.5399.209) [Medline](#)
24. N. Osterman, J. Kotar, E. M. Terentjev, P. Cicuta, Relaxation kinetics of stretched disclination lines in a nematic liquid crystal. *Phys. Rev. E* **81**, 061701 (2010). [doi:10.1103/PhysRevE.81.061701](https://doi.org/10.1103/PhysRevE.81.061701) [Medline](#)
25. A. J. Bray, Theory of phase-ordering kinetics. *Adv. Phys.* **43**, 357 (1994). [doi:10.1080/00018739400101505](https://doi.org/10.1080/00018739400101505)
26. J. Török, S. Krishnamurthy, J. Kertész, S. Roux, Self-quenched dynamics. *Eur. Phys. J. B* **18**, 697 (2000). [doi:10.1007/s100510070017](https://doi.org/10.1007/s100510070017)
27. K. Stratford, R. Adhikari, I. Pagonabarraga, J.-C. Desplat, M. E. Cates, Colloidal jamming at interfaces: A route to fluid-bicontinuous gels. *Science* **309**, 2198 (2005). [doi:10.1126/science.1116589](https://doi.org/10.1126/science.1116589) [Medline](#)
28. L. F. Cugliandolo, J. Kurchan, R. Monasson, G. Parisi, A mean-field hard-spheres model of glass. *J. Phys. A* **29**, 1347 (1996). [doi:10.1088/0305-4470/29/7/007](https://doi.org/10.1088/0305-4470/29/7/007)
29. L. Berthier, G. Biroli, Theoretical perspective on the glass transition and amorphous materials. *Rev. Mod. Phys.* **83**, 587 (2011). [doi:10.1103/RevModPhys.83.587](https://doi.org/10.1103/RevModPhys.83.587)
30. R. S. Jardine, P. Bartlett, Synthesis of non-aqueous fluorescent hard-sphere polymer colloids. *Colloids Surf. A Physicochem. Eng. Asp.* **211**, 127 (2002). [doi:10.1016/S0927-7757\(02\)00258-3](https://doi.org/10.1016/S0927-7757(02)00258-3)
31. D. J. Cebula, J. W. Goodwin, R. H. Ottewill, G. Jenkin, J. Tabony, Small angle and quasi-elastic neutron scattering studies on polymethylmethacrylate latices in nonpolar media. *Colloid Polym. Sci.* **261**, 555 (1983). [doi:10.1007/BF01526620](https://doi.org/10.1007/BF01526620)
32. D. Vollmer *et al.*, Formation of self-supporting reversible cellular networks in suspensions of colloids and liquid crystals. *Langmuir* **21**, 4921 (2005). [doi:10.1021/la047090w](https://doi.org/10.1021/la047090w) [Medline](#)

33. V. Anderson, E. M. Terentjev, Cellular solid behaviour of liquid crystal colloids 2. Mechanical properties. *Eur. Phys. J. E* **4**, 21 (2001). [doi:10.1007/s101890170138](https://doi.org/10.1007/s101890170138)
34. J.-C. Loudet *et al.*, Colloidal structures from bulk demixing in liquid crystals. *Langmuir* **20**, 11336 (2004). [doi:10.1021/la048737f](https://doi.org/10.1021/la048737f) Medline
35. R. Besseling, L. Isa, E. R. Weeks, W. C. K. Poon, Quantitative imaging of colloidal flows. *Adv. Colloid Interface Sci.* **146**, 1 (2009). [doi:10.1016/j.cis.2008.09.008](https://doi.org/10.1016/j.cis.2008.09.008) Medline
36. B. J. Edwards, A. N. Beris, M. Grmela, Generalized constitutive equation for polymeric liquid crystals Part 1. Model formulation using the Hamiltonian (poisson bracket) formulation. *J. Non-Newt. Fluid Mech.* **35**, 51 (1990). [doi:10.1016/0377-0257\(90\)85072-7](https://doi.org/10.1016/0377-0257(90)85072-7)
37. O. Henrich, K. Stratford, D. Marenduzzo, M. E. Cates, Ordering dynamics of blue phases entails kinetic stabilization of amorphous networks. *Proc. Natl. Acad. Sci. U.S.A.* **107**, 13212 (2010). [doi:10.1073/pnas.1004269107](https://doi.org/10.1073/pnas.1004269107) Medline
38. C. Denniston, D. Marenduzzo, E. Orlandini, J. M. Yeomans, Lattice Boltzmann algorithm for three-dimensional liquid-crystal hydrodynamics. *Philos. Trans. R. Soc. London Ser. A* **362**, 1745 (2004). [doi:10.1098/rsta.2004.1416](https://doi.org/10.1098/rsta.2004.1416)